Planetary Defense Conference 2013
Flagstaff, USA

IAA-PDC2013-04-21

Experimental Characterization of the Thrust Induced by Laser Ablation onto an Asteroid

Alison Gibbings[(1)(3)], Massimiliano Vasile[(1)], John-Mark Hopkins[(2)], David Burns[(2)], Ian Watson[(3)]
[(1)] *Advanced Space Concepts Laboratory*, *Department of Mechanical & Aerospace Engineering, University of Strathclyde*, Lord Hope Building, 141 St James Road, Glasgow, G4 0LT, United Kingdom, +44(0)141 548 2326, alison.gibbings@strath.ac.uk, massimiliano.vasile@strath.ac.uk
[(2)] *Institute of Photonics, University of Strathclyde,* Wolfson Centre, 106 Rottenrow, Glasgow, United Kingdom, +44 (0)141 552 4400 john-mark.hopkins@strath.ac.uk, d.burns@strath.ac.uk
[(3)] *Systems, Power and Energy Research Division, School of Engineering, University of Glasgow*, James Watt (South) Building, Glasgow, United Kingdom, +44 (0) 141 330 2032 ian.watson@glasgow.ac.uk

Abstract
This paper presents an improved laser ablation model and compares the performance – Δv and mass efficiency - of laser ablation against contactless deflection methods based on ion-propulsion. The deflection of an asteroid through laser ablation is achieved by illuminating the surface of the asteroid with a high intensity laser light. The absorbed energy induces the sublimation of the surface material and the generation of a plume of gas and ejecta. Similar to a rocket engine, the flow of expelled material produces a continuous and controllable thrust that could be used to modify the trajectory and tumbling motion of the asteroid. Recent results gained from a series of laser ablation experiments were used to improve the sublimation and deflection models. In each experiment a terrestrial olivine sample was ablated, under vacuum, with a 90 W continuous wave laser. The laser operated at a wavelength of 808 nm. The outcomes of the experimental campaign have enabled the mathematic model, and its defining assumptions to be evaluated and updated.

Keywords: *asteroid deflection, laser ablation, ablation model, laser propulsion, asteroid exploitation*

1. Introduction

The contactless manipulation of asteroids removes the requirement for complex landing and surface operations while providing an interesting way to control the trajectory and attitude motion of the asteroid over an extended period of time. Among the techniques for contactless asteroid manipulation, laser ablation has the distinctive advantage of not requiring any extra propellant that is dedicated to providing the variation of the motion of the asteroid. Laser ablation is achieved by irradiating the surface of an asteroid with a laser light source. Part of the energy is absorbed into the asteroid, enabling the illuminated material to sublimate. This transforms the exposed material directly from a solid to a gas. The ablated material then forms into a plume of ejecta that is expelled from the surface. The plume of ejecta then acts against the asteroid, inducing a small, yet continuous low-thrust. It is this low-thrust that can be used to deflect an asteroid from an otherwise impact trajectory with the Earth.

Recently, it has been theoretically demonstrated that asteroid ablation could be achieved with a set of small, low-mass spacecraft, each carrying a solar electric pumped laser system [1][2]. Each spacecraft would fly in formation with the asteroid concurrently producing the sublimation of its surface. The exact number of spacecraft would depend on the size and composition of the asteroid and the warning time before impact. This approach is advantageous as it increases the redundancy, flexibility and scalability of the mission design. Multiple spacecraft also permits the delivery of a much more powerful system. This can be used to reduce the time to achieve a suitable deflection distance. Multiple systems also reduces the risk of any single point failure from occurring. Each spacecraft can be easily replaced from an awaiting unit. A highly redundant mission scenario is preferable as it accounts for large observational uncertainties in the asteroid's material & structural composition and in the mission design parameters [3].

In all previous analyses, the laser ablation model was based on three fundamental assumptions. These assumptions describe the physical formation of the ejecta, the composition of the asteroid and the ejecta's potential to contaminate and degrade any exposed surface that is located within the ablation volume. The first assumption is that the formation of the ejecta plume is similar to the rocket exhaust in standard methods of rocket propulsion. The ejecta plume is therefore limited to the generation of a mono-energetic, friction free compressible gas with no ionization of the gas and any ejection of solid particles. A similar approach is used to model cometary sublimation [10-12]. The second assumption is that the asteroid is a spherical, dense, homogenous body. Forsterite is often used to represent the entire asteroid. It is a compound of MgO and SiO_2

and is therefore classified as the magnesium rich end-members of the olivine solid solution series [13]. Asteroids, however, exist over a diverse range of compositions, geometries and surface features. This includes loose re-accumulated rubble piles, monolithic structures and porous bodies [14][15]. The ablation model must therefore be advanced to represent the diversity within the asteroid population. The third, and final, assumption is that all the ablated material will re-condense on any surface impinging the plume. A layer of deposited material is assumed to remain permanently attached onto the affected surface. Affected surfaces include solar cells, radiators, multi-layering insulation and any optical surfaces and/or device. Optical degradation is considered to follow the Beer-Lambert-Bougier law and is dependent on the optical properties of the deposited layer [17].

The continual accumulation of this deposited ejecta will degrade the system performance of the spacecraft and ablation system. It will affect the power generating ability of the solar arrays and the reflectivity of each mirror or reflective surface. The laser beam power will progressively diminish until the generating thrust will eventually cease completely. Significant degradation will therefore affect the intensity of the laser beam, its operational lifetime and the overall endurance of the ablation technique.

In order to assess the validity of these three assumptions, a series of laser ablation experiments have been performed. A 90 W fibre-semiconductor laser beam, operating at a wavelength of 808 nm, was used to initiate the ablation process. This occurred in vacuum, against a terrestrial rock sample. Olivine was used to represent a rocky, solid asteroid. The results gained from these experiments have been used to update the current mathematic model.

It was found that for a given optical surface, the contamination caused by the ablated ejecta was significantly lower than otherwise predicted in the current laser ablation model. In particular, the density and absorptivity of the deposited material was much lower, while the accumulative thickness was comparable. The deposited material was also loosely bound to the underlying substrate. This material could be easily removed by applying a small vibration and/or an increase in the local surface temperature [4]. The ablation process also resulted in the initial, ejection of small solid particles. This is in addition to the gaseous ejection of material that was similar, although not identical to, the rocket exhaust in standard methods of rocket propulsion. The ejection of solid material appears similar to an explosive event [18][19]. The heating from the laser beam results in the thermal breakdown of material and the build-up of pressure beneath the surface of the target material [18] [20]. The increased pressure combined with imperfections in the target's material, such as voids, cracks, crevices and other surface features, leads to a local fragmentation [18][21].

A further un-modelled effect is the temporal variation in the plume cone angle. Instead a constant scatter factor λ was used to account for the uniform hemispherical, rather than linear expansion of the ejecta plume. This is considered to be a worst-case conservative assumption and will affect the direction and orientation of the resultant thrust vector.

The results of the experiments have led to an improvement in the understanding and modelling of the contamination process [4]. This paper further extends these improvements by including the effects of the energy absorption within the Knudsen layer, the variation of the flow with local pressure and the partial recondensation of the ablated material. The improved ablation model is then used to compare a laser-based deflection action against methods of contactless deflection that is based on ion propulsion.

2. Experimental Results

To improve the ablation model a 90 W continuous wave laser, with a wavelength of 808 nm, operating below the threshold of plasma formation, was used to initiate the ablation events [4]. This occurred within a vacuum chamber with a pump down pressure of $2 \cdot 10^{-5}$ mbar. This therefore provides a more realistic simulation of the laser-to-asteroid ablation event. The experiments enabled the average mass flow rate, plume density and divergence of the ejecta plume to be assessed. Each ablation experiment occurred for 10 minutes and was repeated three times. This aimed to provide more viable and well calibrated data points. Olivine was used to represent a dense, rocky, S-type asteroid. Each sample was shaped into a cube. This enabled the ablation events to occur onto a flat face, which avoided any irregularities cause by the surface material. It therefore provided a tightly focused laser beam onto the surface of the target material. This was also considered to be a realistic analogue of the in-space event, where the spot size of the laser beam would be small in comparison to the size, and major features on the surface of the asteroid. The olivine sample had a density of 3500 kg/m^3, all other material values were assumed from the current literature. This is defined further in Table 1.

The vacuum chamber was surrounded by two cameras and a spectrometer. Each camera was mounted perpendicular to each other and was used to measure the divergence of the ejecta plume. Shown in Figure 1, laser ablation resulted in the hemispheric expansion of a small and extended gaseous plume of ejecta. This was similar, although not identical to, the rocket exhaust in standard methods of propulsion. Laser ablation also resulted in the additional, initial ejection of small, solid particles. The solid ejection of material is not currently accounted for within the numerical model and will contribute to the momentum coupling between the laser and target material. Ablation also resulted in the volumetric removal of material. This is caused by the subsurface excavation of deep and previously inaccessible material, where a small, yet narrow hole extended into the target material. Similar to the rocket exhaust, this would have assisted in focusing the formation of the gaseous plume.

Table 1: Measured and assumed parameters of the olivine asteroid material

Parameter	Value
Bulk Density of the Olivine Sample ρ	3500 kg/m^3
Complete Sublimation Enthalpy of Olivine E_v [22]	14.5·10^6 km/m^3
Black Body Emissivity ε [23]	0.97
Temperature of the target before sublimation T_o	273 K
Heap Capacity C_v [24]	1361 J/kgK
Thermal Conductivity k_{AO} [25]	4.51 W/mK
Gas Heat Capacity C_p [26]	1350 J/kgK
Material Density	3500 kg/m^3

a)   **b)**

Figure 1. Ablation response of the olivine sample: a) initial sublimation stage producing solid particles; b) rocket plume during sublimation of subsurface material.

A spectrometer was also used to measure the inferred temperature of the ablation spot. This was achieved via the Wien's Displacement law by measuring the intensity and wavelength of the emitted spectra. The spectrometer indicated a spot temperature of 4285-4747 K. The velocity of the gases ejecta was calculated by assuming Maxwell's distribution of an idea gas. The velocity of the gaseous ejecta plume was calculated to be ~1131 m/s. Within the vacuum chamber, the olivine sample was mounted on a raised pedestal, at a pre-determined location. This was relative to the known focal point of the laser. The sample was surrounded by a number of highy cleaned microscope slides. These where used as collection plates and were positioned within the ablation volume; 3, 7 or 10 cm away from the known spot location. This was used to measure the mass and height of the deposited ejecta at different points within the plume. It was achieved by measuring the deposited mass per unit area $(\Delta m/A)_{SLIDES}$, where A is the area of each collection plate, and by measuring the thickness of the deposited material Δh_{EXP}. The thickness of the deposited ejecta was measured with a Nikon microscope. Therefore, the density of the deposited material can be computed from:

$$\rho_{EXP}(r,\theta) = \frac{\left(\frac{\Delta m(r,\theta)}{A}\right)_{SLIDES}}{\Delta h_{EXP}} \tag{1}$$

From the model, the expected collection rate of the ejecta on each collection plate can also be derived. This is given as:

$$\frac{1}{A}\frac{dm}{dt} = 2\rho(r,\theta)\bar{v} \tag{2}$$

Equation (2) assumes that the velocity of the expanded gas is ~2 $\overline{v}$. This accounts for the full gaseous expansion into a vacuum and also assumes that all the particles are immediately sticking onto the surface of the collection plate. Mass measurements of the target material before and after each ablation event also enabled the average rate of sublimation to be determined.

Shown in Figure 2 to Figure 4, the accumulated mass per unit area for the three different experiments (i.e. tests) at different distances (either 3,7 or 10 cm) away from the known focal spot locations are shown. The values plotted in the figure correspond to a few discrete, but representative samples that were taken along each collection plate. Each test also produced a different mass flow rate. This is also reported in the figures and is the average value that was experienced over the ablation period of 10 minutes. It can be observed that there is a direct correlation between the amount of deposited ejecta and the ejected mass flow rate. The deposited mass predicted by the model is also very similar to the experiment.

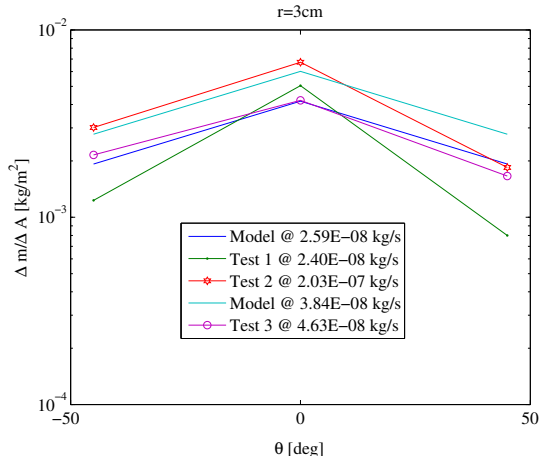

Figure 2. Mass deposits per unit area experimental result vs. model prediction at 3cm from the spot.

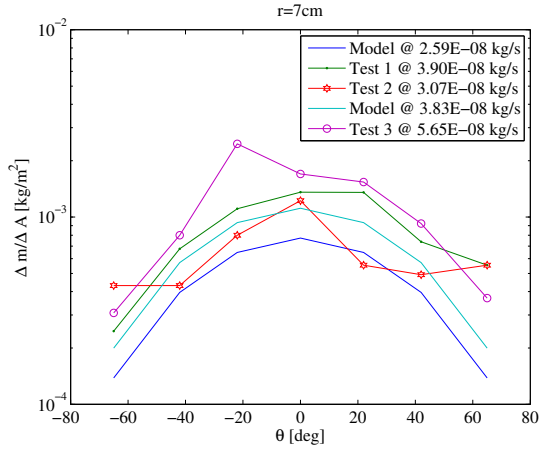

Figure 3. Deposited mass per unit area: experimental result vs. model prediction at 7cm from the spot.

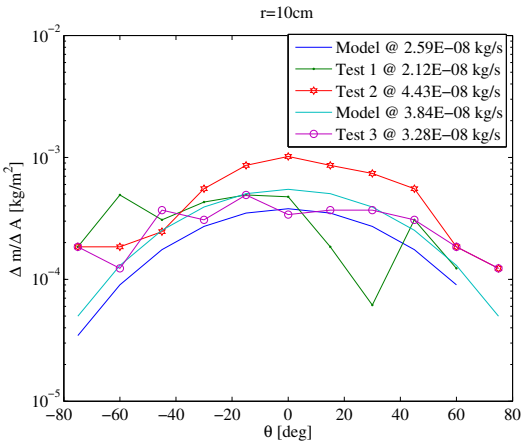

Figure 4. Deposited mass per unit area: experimental result vs. model prediction at 10 cm from the spot.

In comparison, Figure 5 to Figure 7 shows the accumulated thickness of the deposited ejecta. Although the experimental results follow a similar variation with the local elevation angle, the experiment resulted in a much higher thickness, but with an equal mass per unit area. The density of the deposited ejecta on the collection plate is therefore lower than the 1000 kg/m^3 that is currently assumed in the mathematical model [2]. At 7 and 10 cm the average density is ~ 250 kg/m^3. At 3 cm this is much higher with an average value over the central slide of ~ 700 kg/m^3. It is therefore reasonable to assume that at 3 cm from the spot location that the plume is very focused and that the deposited ejecta is mainly distributed over the central slide.

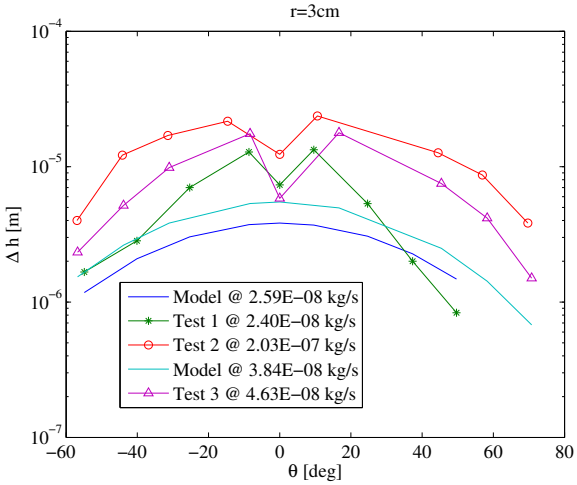

Figure 5. Comparison between the experimental measurements and simulation results for the thickness of the material deposited on the collection plate at 3 cm from the spot.

At 7 and 10 cm from the spot location the plume is more expanded and therefore leads to a more distributed layer of material. In all cases it seems that the model assumes an incorrect growth and density of the deposited ejecta. It also has to be noted that the deposited material is not bonded with the underling substrate of the collection plate. Material can be easily removed by applying a small vibration. The only exception to this occurs at the central point with an elevation angle of zero degrees. This is caused by the self-cleaning action of the laser beam. One possible explanation is that as the laser beam passes through the central collection plate, local heating from the laser beam is causing the re-evaporation of the previously deposited particles. Another possible explanation is that no opaque material re-condenses along the path of the laser beam as it would be constantly excited. Inspected through optical microscopy and the scanning electron microscope, the remains of carbon, oxygen, carbon, magnetism, silicon, chromium, iron and nickel are present with the self-cleaning hole. These are particles that failed to be re-excited by the passing laser beam. The self-cleaning action of the laser beam would serve to increase the system lifetime of any laser ablation system. It also results in more of the laser beam being absorbed by the ablated plume of gas and particles.

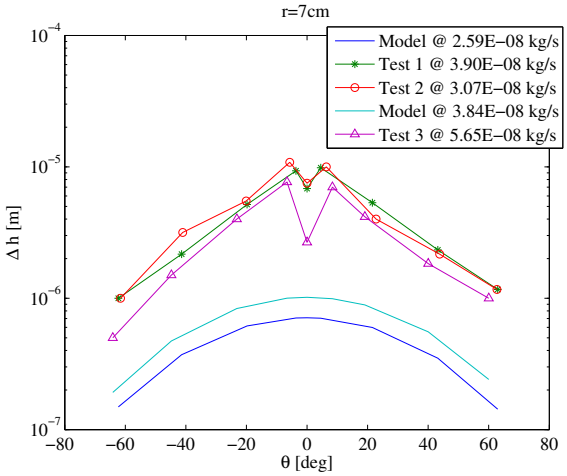

Figure 6. Comparison between the experimental measurements and simulation results for the thickness of the material deposited on the collection plate at 7 cm from the spot.

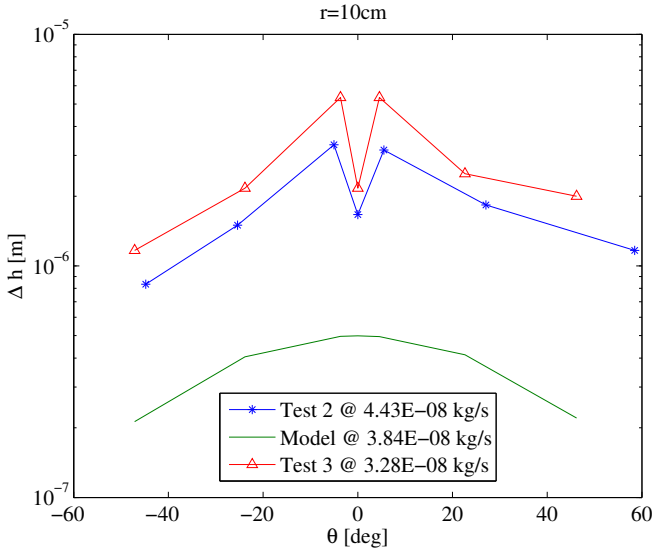

Figure 7. Comparison between the experimental measurements and simulation results for the thickness of the material deposited on the collection plate at 10 cm from the spot.

3. Revised Ablation Model

The revised ablation model, improved from the experimental analysis, derives the mass flow rate per unit area of sublimated material $\dot{\mu}$ from the following one-dimensional energy balance at the illuminated spot.

$$\dot{\mu}\left[E_V + \frac{1}{2}\bar{v}^2 + C_P\left(T_{SUB} - T_0\right) + C_V\left(T_{SUB} - T_0\right)\right] = P_I - Q_{RAD} - Q_{COND} \tag{3}$$

where P_I is the absorbed laser beam per unit area, E_v is the latent heat of complete sublimation, T_{SUB} is the sublimation temperature, T_0 is the temperature of the material prior to sublimation, Q_{RAD} is the heat loss through radiation and Q_{COND} is the heat loss through conduction. The term $C_V\left(T_{SUB} - T_0\right)$ accounts for the energy needed to increase a layer of the target material from the initial temperature T_0 to the sublimation temperature T_{SUB}, whereas the term $\frac{1}{2}\bar{v}^2 + C_p\left(T_{SUB} - T_0\right)$ accounts for the energy that is absorbed by the vapour in the Knudsen layer from the solid-gas interphase (later in the sublimation it is the liquid-gas interface) and the

accelerated phase [26]. Under high, steady-state evaporation a thin layer, immediately adjacent to the evaporating surface is formed. This is known as the Knudsen layer and is created by the gaseous collision of near-surface particles during the initial, high pressure expansion of the plume [28]. From the experimental results, it appears that the additional heat absorbed in the Knudsen layer is equivalent to increasing the enthalpy of sublimation by approximately 1-2·10^6 J/kg. Heating the gaseous ejecta from 3100-4747 k would consume approximately 2 MW/m^2 of energy. This assumes a specific heat of 1361 J/kgK. The specific heat C_v at constant volume is considered to be equal to the maximum heat capacity according to the Debye-Einstein asymptotic heat capacity for solids [24]. While, in comparison, the heat capacity of the gas C_p at constant pressure is the maximum expected heat capacity values given the range of sublimation temperatures of the target material.

The heat losses, per unit area, through conduction Q_{COND} and radiation Q_{RAD} are defined as:

$$Q_{RAD} = \sigma_{SB}\varepsilon\left(T_{SUB}^4 - T_{amb}^4\right) \tag{4}$$

$$Q_{COND} = \left(T_{SUB} - T_0\right)\sqrt{\frac{C_V \rho_A k_A}{\pi t}} \tag{5}$$

The model assumes that the asteroid acts as a black body and emits in the infrared with emissivity ε. In Eq (4) σ_{SB} is the Stefan-Boltzmann constant. The temperature T_{amb} is the ambient temperature which in space is taken to be the background radiation while in the experiment it is the laboratory's ambient temperature. The heat loss through conduction depends on the heat capacity C_V, the density of the material ρ_A and the thermal conductivity k_A. If the target is moving under the spot light, t is the time that the surface of the target is illuminated under the spot light. The hypothesis is that T_0 is constant through the sublimation process and corresponds to the temperature of an infinite heat sink. In this case T_0 of an asteroid is assumed to be its core temperature. The heat conduction from the sublimated material to the inner core is assumed to be a function the sublimation temperature through the relation:

$$k_A = k_{A0}\left(\frac{298}{T_{SUB}}\right)^{0.5} \tag{6}$$

The model considers heat diffusion only from the illuminated spot to the core of the material but not sideways. This component can drain further energy from the ablation process and will be included in a further model. The velocity of the ejecta plume $\overline{v}$ is calculated as the average of the Maxwell's distribution for an ideal gas. This is defined by the sublimation temperature, the molar mass of the ablated material M_a and the Boltzman's constant k_b. It is given by:

$$\overline{v} = \sqrt{\frac{8k_b T_{SUB}}{\pi M_a}} \tag{7}$$

The ablation temperature is related to the local pressure through the Clausius-Clapeyron equation:

$$\ln\frac{p_s}{p_{ref}} = \frac{E_V}{R}\left(\frac{1}{T_{ref}} - \frac{1}{T_{SUB}}\right) \tag{8}$$

where p_s is the pressure corresponding to the temperature T_{sub} and p_{ref} is the pressure corresponding to the reference temperature T_{ref}. The vapour pressure will increase with the temperature of the irradiated asteroid. The reference temperature was taken to be at 1 atmosphere and the enthalpy of complete sublimation is considered to be constant in the range of temperatures in which Eq. (1) is valid.

Previous work has shown that the sublimation temperature of a range of Mg-Fe and Si-Fe oxides can vary from 3175-3800 K [29]. A lower sublimation temperature may also be caused by the transparency of pure minerals [30]. Olivine is a terrestrial rock and can therefore be classified as an inhomogeneous mixture of Fe2Si04, CaAl2Si04, CaMg2Si208 and CaFeSi208, KaAlSi308 and NaAlSi308 [29][31] These additional compounds represent an impurity within the olivine sample and critically will have a different sublimation temperature. This variation will affect the mass flow rate of the ablated ejecta and cause an increase in the local vapour pressure. It will vary on a case-by-case basis and is element and molecule dependent. It is therefore assumed that the reference temperature at 1 atm is T_{ref} = 3800K.

The mass flow rate is also dependent on the local pressure at the interface between the Knudsen layer and the ablated material through the Hertz-Knudsen equation [29][32]. This is expressed as:

$$\dot{\mu} = (1-k)\, p_s \left(\frac{1}{2\pi R_S T_{SUB}} \right)^{\frac{1}{2}} \tag{9}$$

where k is the fraction of molecules that re-condense at the interphase. p_s is the vapour pressure and R_s is the specific gas constant. R_s can be expressed as a function of the molecular mass M_a and the Universal gas constant, R = 8.3144 J/K/Mol where $R_S = R/M_a$. The fraction of molecule that re-condense is expected to increase with the local pressure, however the change in the thrust due to the re-condensation is limited. Figure 8 plots the resulting thrust against the recondensation fraction. The maximum variation is 4% and can therefore be considered negligible.

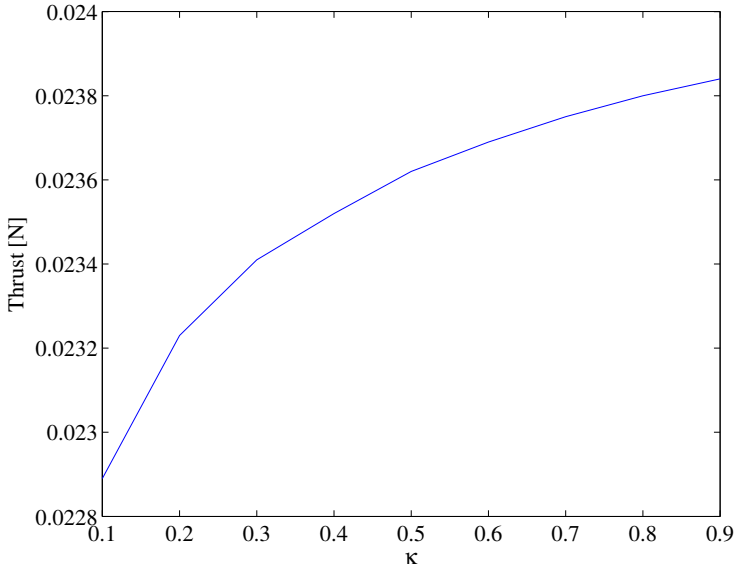

Figure 8. The thrust sensitivity to the recondensation ratio

The experimental results showed that for an olivine sample, the ablated material will dissociate into diatomic oxides. This has a prevalence of SiO and its molar mass is considered to be M_a=0.06 kg/mol. Determined through the scanning electron microscope, the experimental results also showed the incongruent sublimation of the target material. This occurs when the Fe/Mg ratio of the pre-ablated and deposited ejecta is different [32][33][34]. This variation is caused by the chemical breakdown – evaporation, condensation, recombination and decomposition – of the target material [35]. It is achieved by the elemental and isotopic fragmentation of the magnesium and silicon elements and the release of secondary chemical species. This includes, but is not limited to, the gaseous ablation of MgO, FeO, SiO, SiO_2 and O_2. Furthermore as the surface material is ablated away, new underlying material is brought forward. This resulted in the surface enrichment of carbon, sodium, aluminum, chlorine, potassium and calcium. Around the ablation rim, a relatively large layer of semi-melted material is created. This is caused by the thermal propagation of the laser beam and results in the re-crystallization of the original source material. This has the potential to extend the ablation area. The absorbed laser power per unit area P_I is defined as:

$$P_I = \frac{\tau \tau_g \alpha_M \eta_L P_{IN}}{A_{spot}} \tag{10}$$

where η_L is the efficiency of the laser system P_{IN} is the input power to the laser, $\alpha_M = (1-\varepsilon_\alpha \alpha_s)$ is the absorption at the spot and is dependent on the albedo α_s of the asteroid multiplied by the increment in reflectively ε_α at the frequency of the laser beam. For an S-type asteroid the albedo is between 0.1 and 0.3 and has a 20 % reflectivity peak increment between 750 and 800 nm with respect to the central frequency at 505 nm [36]. The revised model also accounts for the absorption of the laser beam τ_g within the rapidly expanding and absorbing plume of gaseous ejecta. It is currently expected, from preliminary experimental results, that the ejecta will absorb 10-15 % of the incoming laser beam. Furthermore, the output power from the laser is

multiplied by a degradation factor τ that accounts for the effect caused by the re-condensed deposited ejected material. The re-condensed material does not directly affect the laser beam but can reduce the power input generated by solar arrays or any other power source that makes use of sunlight.

The degradation caused by the ablated ejecta can also be computed using the model developed in Kahle *et al.* [8].This is determined by first calculating the plume density at a given distance r from the spot location and elevation angle θ from the surface normal. This is illustrated in and is expressed as:

$$\rho(r,\theta) = \rho^* k_p \frac{d_{SPOT}^2}{\left(2r + d_{SPOT}\right)^2}\left[\cos\left(\frac{\pi\theta}{2\theta_{MAX}}\right)\right]^{\frac{2}{k_d - 1}} \tag{11}$$

where d_{SPOT} is the surface spot diameter and the density at the spot ρ^* is given by:

$$\rho^* = \frac{\dot{m}}{A_{SPOT}\bar{v}} \tag{12}$$

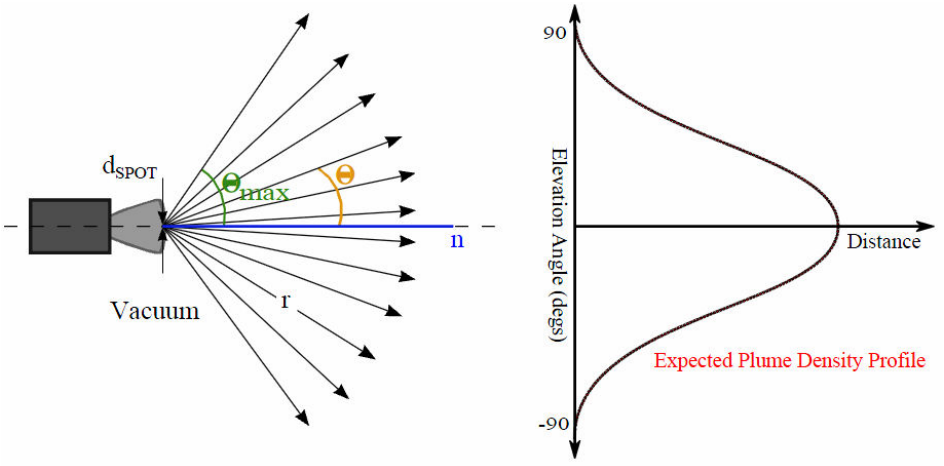

Figure 9. Local reference frame and geometry of the ejecta plume.

For diatomic molecules k_d = 1.44, the jet constant k_p is 0.345 and the expansion angle θ_{max} is limited to 130.45◦ [8]. Following on, the variation of the cumulative ejecta thickness on any exposed surface can be expressed as:

$$\frac{dh}{dt} = \frac{2\bar{v}\rho}{\rho_l}\cos\psi_{vf} \tag{13}$$

This is governed by the velocity and density of the ejecta, the deposition time and the surface properties of the exposed surface. The denominator ρ_l is the layer density. This is the expected density of the deposited material. Based on the experimental results, for an olivine sample this was determined be 250 kg/m^3. The angle Ψvf is the view angle i.e. the angle between the normal to the surface and the surface-to-spot vector. A factor of two is used to account for the estimation of the increase in velocity due to the expansion of gas into a vacuum. Finally the degradation factor τ as given by the Beer-Lambert-Bougier-law can be expressed as:

$$\tau = \exp^{-2\eta h} \tag{14}$$

where η is the absorbance per unit length of the accumulated ejecta and h is the thickness of the deposited material. A factor of two is used to account for the double passing of the surface layer. Photons will have to transverse the contaminated layer, be reflected and then transverse the ejecta layer for a second time [8][16]. This degradation factor is applied to the power density initially beam onto the surface of the asteroid. From experiments, the absorbance per unit length for an ablated olivine sample is $5 \cdot 10^4$ m^{-1}.

According to the model developed in Sanchez *et al* 2009 [7], the mass flow can be computed by integrating $\dot{\mu}$ over the surface area illuminated by the laser beam:

$$\dot{m} = 2V_{ROT} \int_{y_{\min}}^{y_{\max}} \int_{t_{in}}^{t_{out}} \frac{1}{E_v^*} \left(P_I - Q_{RAD} - Q_{COND} \right) dydt \tag{15}$$

The term $\left(E_v + \frac{1}{2}\bar{v}^2 + C_p\left(T_s - T_0\right) + C_v\left(T_s - T_0\right) \right)$ can be seen as an augmented enthalpy, called E_v^*. Furthermore the limit [y_{min}, y_{max}] and [t_{in}, t_{out}] define the location and duration for which the surface spot is illuminated respectively. The two quantities [t_{in}, t_{out}] are the times at which the asteroid's surface moves inside and out of the illuminated spot. V_{rot} is the velocity of the asteroid as it travels through the illuminated spot area.

The force action on the asteroid F_{sub} can then be computed by the product of the ejecta velocity and mass flow rate of the ablated material:

$$F_{SUB} = \lambda \bar{v} \dot{m} \tag{16}$$

where λ is the scatter factor as the integral of the trigonometric part in Eq (11).

4. Simulation Results

The revised model can be used to evaluate the ability of laser ablation to deflect a small size asteroid over an extended period of time. The metric to evaluate the performance of laser ablation is the total imparted Δv. This is defined as: $\Delta v = \int_{t_i}^{t_f} \frac{F_{SUB}(t)}{m_A(t)} dt$ where $\Delta t = t_f - t_i$ is the total actual sublimation time and m_A is the mass of the asteroid. The material properties of asteroid were assumed based on the values previously given in Table 1. In the analysis the maximum total sublimation time was set to 10 years and the Δv was computed for different power inputs to the laser, spot sizes and distances between the spot and the laser. The last parameter has an impact on the actual sublimation time. The effect of contamination can reduce the surface power density below the sublimation limit.

Figure 10 and Figure 11 shows the imparted Δv as a function of the input power to the laser and spot radius. The initial mass of the asteroid is $m_A = 1 \cdot 10^9$ kg. This corresponds to a 42 m in radius asteroid with an average density of ~ 3500kg/m^3 and one rotation per day. The analysis, as shown in Figure 11, reveals that a longer distance is preferable; however the distance from the spot has an impact on the size of the optics that is required to focus the laser beam. For example, a 1.5 mm spot at 500 m would require a focusing mirror with a diameter of 430 mm. The same spot size at 250 m would require a focusing mirror with a diameter of 210 mm. This reduction is advantageous in reducing the mass of the optical system. A 100 mm in diameter mirror would require 10 kg of optics. This is based on system design considerations reported in Vasile *et al.,* 2013 [37]. Assuming that the mass of the optics can be scaled to the area of the mirror, then a 201 mm in diameter mirror would have an optical mass of 44 kg. A 430 mm in diameter mirror would have an optical mass of 185 kg.

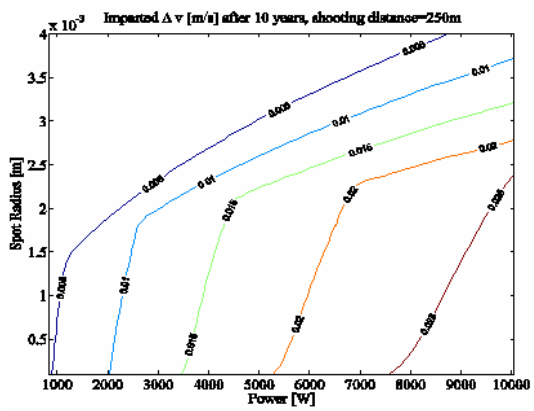

Figure 10. Imparted Δv as a function of spot size and input power to the laser 250 m distance from the spot.

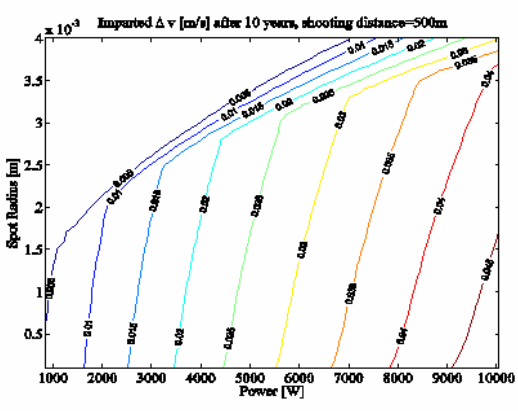

Figure 11. Imparted Δv as a function of spot size and input power to the laser 500 m distance from the spot.

Performance can also be evaluated by the mass efficiency of the laser ablation system. The mass efficiency defines the mass of the deflection system that is required to obtain a given Δv. The mass of the laser system m_{LS} can be estimated as:

$$m_{LS} = \alpha_P P_{IN} + \rho_R A_R (1-\eta_L) \frac{P_{IN}}{\sigma \varepsilon_R T_R^4} + m_L \tag{17}$$

where m_L is the mass of the laser itself plus the optics, ρ_R = 0.5 kg/m^2, is the mass of the radiators, ε_R their emissivity, T_R their operating temperature, A_R their area, α_P is the specific mass of the power system, P_{IN} is the input power to the laser, η_L is the efficiency of the laser that is assumed to be 55% in this analysis. The specific mass of the power system, which derived again from system level considerations, is 40 kg/W and the mass of the laser is 10 kg/kW [37] This assumes that the heat sink is included in the thermal control system, i.e. the radiators. The temperature of the radiators is assumed to operate at the temperature at which the diodes of the laser need to function. This is 283 K and the emissivity was taken to be 0.8. The input power is assumed to be generated by a set of solar arrays and is therefore given by:

$$P_{IN} = \eta_P \eta_S \frac{P_{1AU} A_{SA}}{R_{AU}^2} \tag{18}$$

where A_{SA} is the area of the array, R_{AU} is the distance from the Sun in Astronomical Units (AU), P_{1AU} is the power per square meter at 1AU, η_P is the efficiency of the power system and η_S the efficiency of the solar arrays. For comparison the mass efficiency of the laser system can be compared to the mass efficiency of an electric propulsion (EP) system that produces the same Δv. The mass of the EP system should include the mass of two engines (whether it is an ion beaming system or a gravity tractor), the mass of the related power system, the mass of the radiators, the mass of propellant and the mass of the tanks. The mass of the radiator and power system is computed using the same figures and assumptions used for the laser system except for the efficiency of the engine that is always equal to 60 %. This is a rather optimistic assumption as the efficiency does not scale with the thrust level. The mass of the propellant is simply $m_p = 2F_{EP}\Delta t_{thrust} / I_{sp} g_0$, the mass of the EP system is therefore:

$$m_{EP} = 2.2 \frac{F_{EP}}{g_0 I_{sp}} \Delta t_{thrust} + \alpha_P P_{IN} + \rho_R A_R (1-\eta_{EP}) \frac{P_{IN}}{\sigma \varepsilon_R T_R^4} + 2m_e \tag{19}$$

where m_e is the mass of a single engine, I_{sp} is the specific impulse of the engine and η_{EP} is the efficiency of the EP system that is assumed to be 60 % in this analysis. The assumptions here are that the mass of the tanks is only 10 % of the mass of the propellant. Furthermore, the transfer of momentum is considered to be equal to one, which corresponds to an ideal ion beaming system. The specific impulse in this comparison is taken to be 3500s. The mass of the engine is assumed to be 5kg/kW. This excludes electronics and the PDCU, which are assumed to be included in the power system.

Figure 12 shows the mass of the laser system (LS), assuming a spot size of 1mm and a distance of 250m, versus the mass of the asteroid. The optics does not change with the power as the distance and spot size are constant, therefore one can add a fixed mass equal to 100kg corresponding to a 160mm optics to the mass of the deflection system. Figure 13 shows the mass of the EP system with the same input power of the laser system and delivering the same Δv. In order to have a correct and fair comparison of the two concepts it is assumed that the thrust of the EP system follows the same profile of the thrust of the LS system and is on for the same length of time. The difference in mass is mainly due to the propellant consumption and associated tanks.

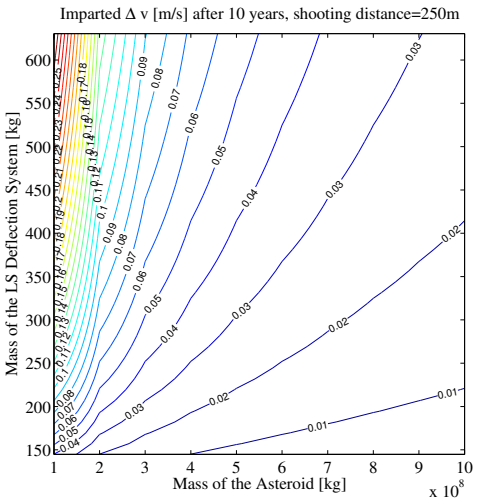

Figure 12. Imparted Δv of laser ablation as a function of asteroid mass and mass of the deflection system.

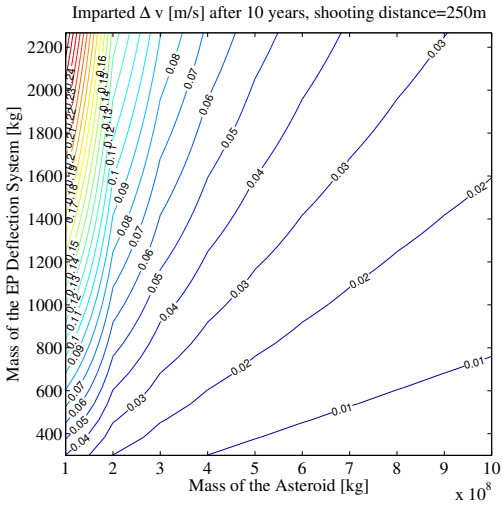

Figure 13. Imparted Δv of ion propulsion system as a function of asteroid mass and mass of the deflection system.

These two graphs demonstrate that for the same installed power and for the same resulting Δv the laser system is more advantageous. For any ion beaming technique a higher Δv, at a given installed power, can only be achieved by increasing the onboard propellant mass. This has a consequential increase in the deflection system mass and complexity (higher structural mass, higher piping and harness mass, etc.). This is not an issue for laser ablation. The propellant to sustain the defection action is provided for free by the direct ablation of the asteroid.

On the other hand, an increase in the efficiency of ion engines could potentially allow a faster deflection with the same overall system mass. At the same time the laser system needs to cope with the contamination that can be higher than the model predicts and with the actual energy efficiency of the ablation process that can be lower than expected if a three dimensional heat diffusion model is considered. This last point is the subject of current investigation.

5. Final Remarks

This paper has proposed an updated ablation model based on experimental results. Some critical assumptions have been validated or updated and new parameters have been included in the model. The model of energy absorption within the target material has been revised and a model for the formation of the Knudsen layer and recondensation of the ablated material has been included in the deflection model. By using this updated deflection model one can argue that laser ablation can achieve better performance than ion-engine based techniques at the deflection of small to medium scale asteroids. It was demonstrated that in the range of asteroid masses considered in this paper that the Δv and mass efficiency of the laser system are always advantageous when compared to other contactless methods of asteroid deflection. However further work – experimental and analytical – is still required. This includes more detailed and inclusive ablation experiments. This will directly measure the mass flow rate and temperature of the ejecta plume and the orientation of the resultant thrust vector. These issues will be addressed to further, planned experiments. It is also important to understand the three dimensional energy balance of sublimation, the effects of a de-focused laser beam and the reduction of laser energy during the lifetime of the mission.

Acknowledgements

This study is partially supported by the Planetary Society.

References

[1] Vasile M., Maddock C., Summerer L., Conceptual Design of a Multi-Mirror System for Asteroid Deflection. 27th International Symposium on Space Technology and Science, 5-12 July 2009, Tsukuba, Japan.

[2] Vasile M., Maddock C., Design of a Formation of Solar Pumped Lasers for Asteroid Deflection, Advances in Space Research, Volume 50, Issue 7, 1 October 2012, Pages 891–905.

[3] Zuaini F., Vasile M., Gibbings A., Evidence-Based Robust Design of Deflection Actions for Near Earth Objects, Celestial Mechanics and Dynamical Astronomy, July 2012, DOI 10.1007/s10569-012-9423-1.

[4] Gibbings A, Vasile M, Watson I, Hopkins J-M, Burns D, Experimental Analysis of Laser Ablated Plumes for Asteroid Deflection and Exploitation, Acta Astronautica. (2012) http://dx.doi.org/10.1016/j.actaastro.2012.07.008.
[5] Phipps CR, Luke J.R Advantages of an ns-pulse Micro-laser Plasma Thruster, In Beamed Energy Propulsion: APS Conference Proceedings, Institute of Physics. 1 (2003) 230-239
[6] Phipps CR, Reilly JP, Campbell JW, Optimum Parameters for Launching Objects into Low Earth Orbits, Laser and Particle Beams. 18 (2000) 661-695
[7] Sanchez Cuartielles, J. P., Colombo, C., Vasile, M., and Radice, G., Multi-criteria comparison among several mitigation strategies for dangerous near earth objects, Journal of Guidance, Control and Dynamics 32 (2009): 121-142.
[8] Kahle R, Kuhrt E, Hahn G, Knollenberg J, Physical Limits of Solar collectors in Deflecting Earth-threatening Asteroids, Aerospace Science and Technology. 10 (2006) 256-263
[9] Phipps CR, Michaelis MM, Laser Impulse Space Propulsion. Laser and Particle Beams. 54, (1994) 12-23
[10] Kimura H, Mann I, Jessberger EK. Dust Grains in the Comae and Tails of Sungrazing Comets: Modelling of their Mineralogical and Morphological Properties, Icarus. 159 (2002), 529-541.
[11] Mohlmann D, Cometary Activity and Nucleus Modelling: A New Approach, Planet SpaceScience. 44 (1996) 541-546,1996
[12] Crifo J.F, A General Physicochemical Model of the Inner Coma of Active Comets: Implications of Spatially Distributed Gas and Dust Production. Astrophysical Journal. 445 (1995) 470-488
[13] Hashimoto A, Evaporation Metamorphism in the Early Solar Nebula Evaporation Experiments on the Melt FeO-MgO-Si02-CaO-Al203 nd Chemical Fractionations of Primitive Materials, Geochemical Journal. 17 (1983) 111-145
[14] Huebner WF, Greenberg JM, Methods of Determining Strength and Bulk Properties of NEOs, Advanced Space Research. 28 (2001) 1129-1137
[15] O'Brien D and Greenberg JM, The Collisional and Dynamical Evolution of the Man-belt and Nea size distributions, Icarus 178 (2005)179-212
[16] Tribble AC, Fundamentals of Contamination Control (SPIE Tutorial Text in Optical Engineering Vol. TT44) 1961 ISBN-10: 0819438448
[17] Matteson s, Particulate Contamination in Atomic and Molecular-beam Deposition System, Vacuum Science and Technology A - Vacuum, Surfaces and Films. 6 (1988) 2504-2507
[18] Domen K, Chuang TJ, 1 Laser Induced Photodissociation and Desorption. II. CH2I2 Adsorbed on Ag, Journal of Chemistry Physics. 90 (1989) 3332-3338
[19] Kelly R, Miotello A, Comments on Explosive Mechanisms of Laser Sputtering, Applied Surface Science. 96 (1996) 205-215
[20] Vidal F, Johnston TW, Laville S, Barthelemy M, Chaker M, Le Drogoff B, Margot J, Sabsabi M Critical-Point Phase Separation in Laser Ablation of Conductors Physical Review Letters. 86 (2001) 2573-2576
[21] Clauser C, Huenges E, Thermal Conductivity of Rocks and Minerals, Rock Physics and Phase Relations, T.J Ahrens (Ed), American Geophysical Union.1 (1995) 105-126
[22] G. Dettleff, Plume flow and plume impingement in space technology, Aerospce Science. 28 (1991) 1–71.
[23] M.M. Marinova, O. Aharonson, E. Asphaug, Geophysical conse- quences of planetary-scale impacts into a Mars-like planet, Icarus 211 (2011) 960–985
[24] Robbie R.A., Hemingway B.S., Takei H. Heat Capacities and Entropies of Mg_2SiO_4, Mn_2SiO_4 and Co_2SiO_4 between 5 and 380K, American Mineralogist. 67 (1982) 470-482
[25] J. Lindgrad, K. Jonansen, Production and Testing of Concrete with High Specific Heat, P. Bartos, D.L. Marrs, D.J. Cleland (Eds.) In: Proceedings of the International RILEM Conference, Paisley, Scot- land, June 3–5 1996
[26] Knight CJ, Theoretical Modeling of Rapid Surface Vaporization with Back Pressure, AIAA. 15 (1979) 519-523.
[27] Kelly R, Dreyfus R.W, Reconsidering the Mechanisms of Laser Sputtering with Knudsen-layer Formation Taken into Account, Nuclear Instruments and Methods in Physics Research Section B: Beam Interactions with Materials and Atoms. 32 (1988) 341-348.
[28] Bulgakov AV, Bulgakova NM, Thermal Model of Pulsed laser Ablation under the Conditions of Formation and Heating of a Radiation-Absorbing Plasma, Quantum Electronics. 29 (1999) 433-437
[29] O'Keefe J.D, Ahrens T.J, Shock Melting and Vaporisation of Lunar Rocks and Minerals Conference on Lunar Geophysics, Lunar Science Institute in Houston, Texas, U.S.A, October 18-21 1971
[30] Hagahara H, I Kushiro Mysen BO Olivine at Low Pressures and its Implications for the Origin of Chondrules, Lunar Planetary Science Conference XXIII. 23 (1992) 959-960
[31] Farqyhar and Rumble, Comparison of Oxygen Isotope Data Obtained by Laser Fluorination of Olivine with KrF Excimer Laser and CO2 laser, Geochimica et Cosmochimica Acta. 62 (1998) 3141–3149

[32] Nagahara H, Kushiro I, Mysen BO. Evaporation of Olivine: Low Pressure Phase Relations of the olivine System and its Implications for the Origin of Chondritic Components in the Solar Nebula, Geochimica et Cosmochimica Acta. 58 (1994) 1951-1963
[33] Nagahara H, Kushiro I, Mori H, Mysen BO, Experimental Vaporisation and Condensation of Olivine Solid Solution, Nature. 331 (1988) 516-518
[34] Nagahara H, Kita N.T, Ozawa K, Morishita Y, Condensation of Major Elements During Chondrule Formation and its Implications to the Origin of Chondrules, Geocimica et Cosochimica Acta. 72 (2009) 1442-1465
[35] Hashimoto A, Evaporation Kinetics of Forsterite and Implications for the Early Solar Nebula, Nature. 347 (1990) 53-55
[36] Bus SJ, Vilas F, Barucci MA, Visible-wavelength Spectroscopy of Asteroids. Asteroids III. 1 (2002)169-182.
[37] Vasile M, Gibbings A, Vetrisano M, Yarnoz D, Cuartielles JP, McInnes C, Burns D, Hopkins JM, Colombo C, Branco J, Wayman A, Eckersley S, Light-Touch2: A Laser-Based Solution for the Deflection, Manipulation and Exploitation of Small AsteroidsIAA-PDC13-04-22, Planetary Defense Conference 2013, Flagstaff, USA